

Communication

Measurement of the Temperature Dependence of Polarization Switching in Gain-Switched VCSELs for Quantum Random Number Generation

Iván Rivero, Alfonso Lázaro del Pozo, Marcos Valle-Miñón, Ana Quirce  and Angel Valle 

Instituto de Física de Cantabria (CSIC-Univ. Cantabria), Avda. Los Castros s/n, E39005 Santander, Spain; ivan.rivero@alumnos.unican.es (I.R.); alfonso.lazaro@alumnos.unican.es (A.L.d.P.); marcos.valle@alumnos.unican.es (M.V.-M.); quirce@ifca.unican.es (A.Q.)

* Correspondence: valle@ifca.unican.es; Tel.: +34-942201465

Abstract: We report an experimental study of the effect of the temperature of the VCSEL on the probability of excitation of a linearly polarized mode when gain-switching the device. We consider different modulation frequencies and amplitudes. We show that the probability of excitation of a linearly polarized mode significantly changes with the value of the temperature of the device. We also show that for low values of the temperature the probability of excitation saturates to a constant value as the amplitude of the modulation increases. This extends our previous results obtained at larger temperatures for which that saturation was not observed. We identify situations in which the distributions of the linearly polarized signals at a sampling time are approximately uniform. For these cases we evaluate the quality of the random numbers by using statistical test.

Keywords: semiconductor laser; VCSEL; gain-switching; spontaneous emission noise; quantum random number generation



Citation: Rivero, I.; Lázaro del Pozo, A.; Valle-Miñón, M.; Quirce, A.; Valle, A. Measurement of the Temperature Dependence of Polarization Switching in Gain-Switched VCSELs for Quantum Random Number Generation. *Photonics* **2023**, *10*, 474. <https://doi.org/10.3390/photonics10040474>

Received: 23 March 2023

Revised: 18 April 2023

Accepted: 18 April 2023

Published: 20 April 2023



Copyright: © 2023 by the authors. Licensee MDPI, Basel, Switzerland. This article is an open access article distributed under the terms and conditions of the Creative Commons Attribution (CC BY) license (<https://creativecommons.org/licenses/by/4.0/>).

1. Introduction

Theoretical and experimental understanding of the fluctuations of laser light began shortly after the invention of the laser [1–5]. Special attention has been paid to fluctuations of the light emitted by semiconductor lasers [6–9] due to their vast variety of applications. In most of these applications the effect of laser noise is detrimental. For instance, spontaneous emission noise causes enhancement of the lasing optical spectrum [8], timing jitter fluctuations during the laser turn-on [10–12], or random excitation of different longitudinal lasing modes [13]. However, novel applications are emerging in which the fluctuating character of laser light is beneficial. One example is the random number generation (RNG) using semiconductor lasers.

Random numbers are a vital resource for numerous applications, including cryptography, Monte Carlo simulations, quantitative finance, massive data processing, etc. [14–16]. Quantum random number generators (QRNGs) stand out from RNGs because their randomness stems from quantum processes, this being the best guarantee for offering optimum privacy and security while maintaining high performance [15,16]. QRNG have advantages in quantum computation and quantum communications [17–22]. QRNGs have emerged as certifiable source of true random numbers, being basic elements in practical quantum key distribution (QKD) systems [23]. Device-independent randomness expansion using entangled photons [24] and source-independent QRNGs [25] have been recently demonstrated. QRNGs based on the detection of single-photon events [26–30] and multiphoton QRNGs [31–47] have been demonstrated.

One of the most common multiphoton techniques for QRNG is based on the phase fluctuations of the light emitted by pulsed semiconductor laser diodes [34,37–40,43,45]. These fluctuations are caused by spontaneous emission photons. Spontaneous emission

is a useful mechanism to generate quantum fluctuations, as it can be ascribed to the vacuum fluctuations of the optical field [34,48]. In these QRNGs, light pulses with similar amplitudes and randomized phases are generated by repetitive gain-switching of a single-mode semiconductor laser from below to above its threshold. One way of converting those phase fluctuations into amplitude fluctuations is by using an unbalanced Mach–Zehnder interferometer. From these amplitude fluctuations, random numbers are obtained after proper digitization. Advantages of this type of generators include simplicity, fast operation at Gbps rates (up to 68 Gbps [39]), robustness, low cost, multiclock frequency flexibility, and full integration on an InP platform [40]. Gain-switched single-mode semiconductor lasers and QRNGs based on this system have been recently used for state preparation in QKD [23,49].

Gain-switching of multimode semiconductor lasers, in particular vertical-cavity surface-emitting lasers (VCSELs), has also been used for QRNG. VCSELs usually show two orthogonal linearly polarized modes in such a way that polarization switching (PS) between them can be observed when changing the bias current or the temperature of the device [50,51]. When the VCSEL's bias current is modulated from below to above the threshold value, the linear polarization mode that is preferably excited is random because it is determined by the sequence of spontaneous emission noise events. This randomness is the basis of the QRNGs using gain-switched VCSELs that have been proposed [46,52–56]. QRNGs based on VCSELs have the advantages of low fabrication costs, small size, compactness, and simplicity (coherent detection is not required). VCSELs also offer advantages such as on-wafer testing capability, fast operation, high energy efficiency, and ease of 2D array packaging [51].

Using VCSEL's polarization behavior for random number generation was firstly proposed by Chizhevsky [52]. He experimentally demonstrated random bit generation of up to 2 Mbps by using the polarization bistable behavior arising in some of the PS in VCSELs [52]. Polarization bistability has also been used in subsequent theoretical analysis [53,54,56]. Although bistable operation is desirable for obtaining that, given a particular pulse, most of the total power is emitted in one of the two linearly polarized modes, it can be a drawback if we want to achieve unbiased operation of the QRNG (that is, equal probability for “0” and “1” generated bits). In fact, equal probability of occurrence of pulses with orthogonal polarizations has only been obtained for specific values of some internal laser parameters: the photon lifetime and the linear birefringence [54] or different fractions of spontaneous emission noise coupled to each polarization mode [53]. One simple way of obtaining similar probabilities of excitation of both linearly polarized modes was experimentally achieved by adjusting the modulation conditions and the sampling time in a VCSEL having PS under continuous wave operation [55]. This VCSEL has a very narrow bistable region, so bistable operation is not essential for generating random numbers when gain-switching this device [55]. In fact, a QRNG based on the random excitation of the linearly polarized modes of this gain-switched VCSEL was experimentally demonstrated [46]. In [46], we obtained a large random bit stream that, after appropriate post-processing, fully passed all tests in the standard test suite for RNGs provided by the National Institute of Standards and Technology (NIST) [57].

It has been shown that the laser substrate temperature has a large impact on the polarization properties of VCSELs, and in particular on the PS of VCSELs [50,51,58,59]. This is due to the large effect of the temperature on the laser parameters determining the VCSEL's polarization, such as material gain, optical losses, effective dichroism, and nonlinear dichroism [50,51,58,59]. It is therefore expected that the temperature has a large impact on the probability of excitation of a linear polarization mode when gain-switching the VCSEL, affecting, then, the characteristics of QRNGs based on this system. In this paper, we perform a systematic experimental analysis of the effect of the temperature on the linear polarization mode emitted by the VCSEL when modulating the bias current from below to above the threshold value. Different modulation frequencies and amplitudes are considered in our analysis. We show that for low values of the temperature, the probability

of excitation of a linearly polarized mode saturates to a constant value as the amplitude of the modulation increases. This extends our previous results obtained at larger temperatures in which that saturation was not observed [55]. We also identify modulation conditions and sampling times for which the distributions of the signals for each linearly polarized mode are approximately uniform. This situation is of interest because a minimum post-processing of the raw data when using the system for QRNG would be expected. Evaluation of the quality of the randomness of the numbers distributed in that way is performed by using NIST statistical test.

The paper is organized as follows. In Section 2 we describe the experimental setup and the device characterization. Section 3 is devoted to describing the dependence of the probability of excitation of a linearly polarized mode in gain-switched VCSELs on the temperature of the device. Finally, in Section 4, a discussion and a summary are presented.

2. Experimental Setup and Device Characterization

The experimental setup is shown in Figure 1. A quantum-well long-wavelength (1550 nm) VCSEL (RayCan) is used in the experiments. The same device was used in [46,55]. The laser is mounted in a laser mount that includes a bias-tee. The VCSEL is gain-switched by applying a superposition of two electrical signals: a constant bias current (I_{off}) and an RF square signal provided by a pulse pattern generator. The control of the temperature of the VCSEL is performed using a temperature controller. An optical isolator (OI) is used to minimize optical feedback effects in the laser. A polarization controller (PC) and a polarization beamsplitter (PBS) are used to separate the two linearly polarized modes of the VCSEL. Two fast-photodiodes (9 GHz bandwidth) are used to detect the signal corresponding to each linearly polarized mode. These signals are recorded in a real-time oscilloscope (13 GHz bandwidth) to obtain the temporal profiles of the power of each linearly polarized mode. A more detailed description of the elements of the setup can be found in [55].

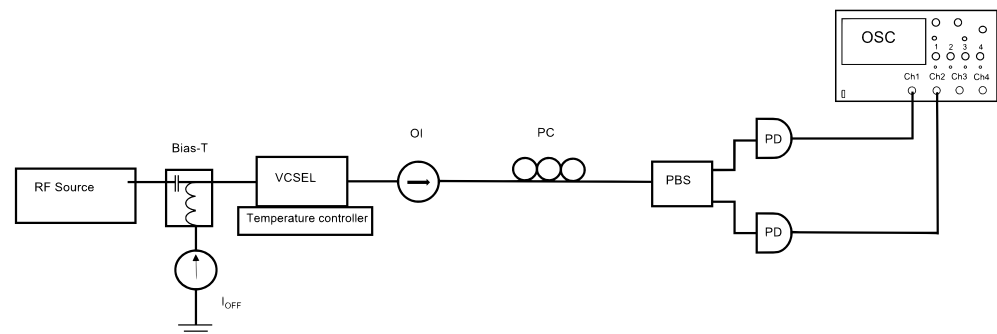


Figure 1. Experimental setup. OI: optical isolator, PC: polarization controller, PBS: polarization beam splitter, PD: photodetector, OSC: oscilloscope.

The VCSEL operates in a single transverse and longitudinal mode over the whole bias current range. However, the emitted polarization changes when changing the bias current, as shown in Figure 2. This figure shows the polarization-resolved light–current curve for two different temperatures of the VCSEL. PS from the short-wavelength (labeled as y) to the long-wavelength (x) linearly polarized mode is observed for both temperatures. The optical frequency splitting between the y and the x linear polarizations is 29.8 GHz [55]. The current at which the PS is observed slightly decreases when increasing the temperature (from 6.81 mA at $T = 20\text{ }^{\circ}\text{C}$ to 6.73 mA at $T = 25\text{ }^{\circ}\text{C}$).

Narrow polarization hysteresis cycles are observed: PS is observed at 6.38 mA and 6.50 mA when decreasing the bias current in Figure 2a,b, respectively. The width of bistable regions are 0.43 and 0.23 mA for $T = 20\text{ }^{\circ}\text{C}$ and $T = 25\text{ }^{\circ}\text{C}$, respectively. The threshold current of the VCSEL, I_{th} , slightly increases with the temperature: I_{th} changes from 2.39 mA ($T = 20\text{ }^{\circ}\text{C}$) to 2.51 mA ($T = 25\text{ }^{\circ}\text{C}$). In this work we will consider $I_{off} = 0.92I_{th}$,

since a switch-off bias current value below the threshold is required for the VCSEL to operate as a QRNG.

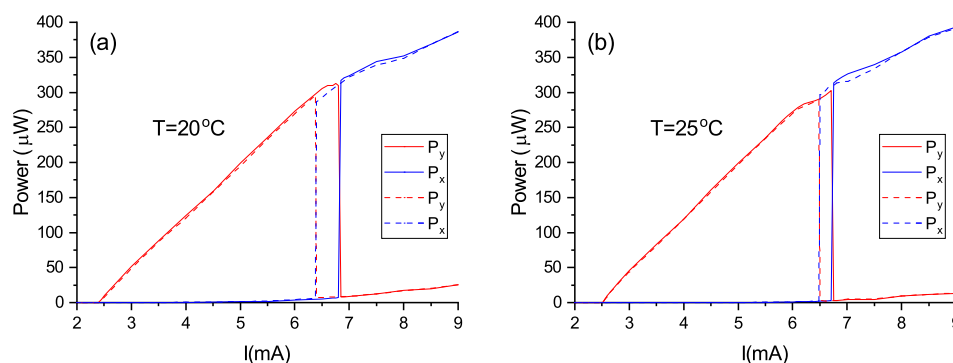


Figure 2. Polarization-resolved light–current characteristics when increasing (solid lines) and decreasing the current (dashed lines) for a temperature of (a) 20 °C and (b) 25 °C.

3. Experimental Results

A square wave modulation is applied to our VCSEL in which I_{off} is below the threshold value during $P/2$, and a voltage pulse of constant amplitude V_{on} is applied during the rest of the period, P . The temporal waveforms of the x - and y -signals measured at the oscilloscope, V_x and V_y , are shown in Figure 3a when the temperature is 20 °C, $I_{off} = 2.2$ mA, $V_{on} = 0.4$ V. The modulation frequency, f_{mod} , is 100 MHz since $P = 10$ ns. The signal corresponding to the total power, $V_x + V_y$, is also shown in the figure. The VCSEL switches off in all the periods in such a way that there is a random excitation of both linear polarization modes induced by spontaneous emission noise. The total power fluctuates much less than the individual linear polarizations [55,60]. One way of obtaining random numbers from the fluctuations of both linear polarizations is by regularly sampling the x - and y -signals at a sampling time, t_s , measured with respect to the beginning of each modulation cycle, that is, the time at which V_{on} is applied ($t = 0$ in the figure for the first cycle). In this way, for the m cycle, the signals are sampled at $t_m = t_s + mP$, where $m = 0, 1, \dots$ is an integer. We show in Figure 3a, with symbols, the signals sampled with $1/P$ frequency, $V_x(t_s)$ and $V_y(t_s)$. The comparison between $V_x(t_s)$ and $V_y(t_s)$ is one way to determine the obtained random bit. We considered that if $V_x(t_s) > V_y(t_s)$ ($V_x(t_s) \leq V_y(t_s)$) then we obtain a “0” (“1”) bit, similarly to [55].

Figure 3b shows the the probability density functions (pdfs) of the x - and y -polarized signals at $t_s = 3.35$ ns. These normalized histograms are obtained with 10^4 data. The temperature of the VCSEL is different to that considered in [55]. In addition, the modulation parameters and sampling time were chosen in order to obtain pdfs of $V_x(t_s)$ and $V_y(t_s)$ with a shape closer to that corresponding to a uniform distribution. This contrasts with the shapes obtained in [55] in which both pdfs had clear local maxima close to the maximum and minimum values of the signals in such a way that the probability of obtaining values in the central part of the histograms was low.

In order to analyze the effect of the temperature on our system, we consider the probability of excitation of the x -polarization, $P(X > Y)$, as the probability of obtaining $V_x(t_s) > V_y(t_s)$, that is, the probability of obtaining a “0” bit. As an example, $P(X > Y) = 0.501$ for the case analyzed in Figure 3. In [55], we analyzed the dependence of $P(X > Y)$ on the amplitude of the voltage pulse. We found that $P(X > Y)$ increases with V_{on} for the considered operation temperature, $T = 25$ °C. This is also shown in Figure 4, in which $P(X > Y)$ is shown as a function of V_{on} for $T = 25$ °C. However, the situation changes when decreasing the value of T , as can be seen in Figure 4 for the case of $T = 20$ °C. After an initial increase of $P(X > Y)$ when V_{on} is small, a clear saturation of the values of $P(X > Y)$ is obtained for a very wide range of values of V_{on} . We also note that the change of $P(X > Y)$ when the temperature changes in 5 °C can be very large. For instance, for $V_{on} = 0.6$ V, $P(X > Y)$ decreases from 0.641 to 0.361 when T changes from 20 °C to 25 °C.

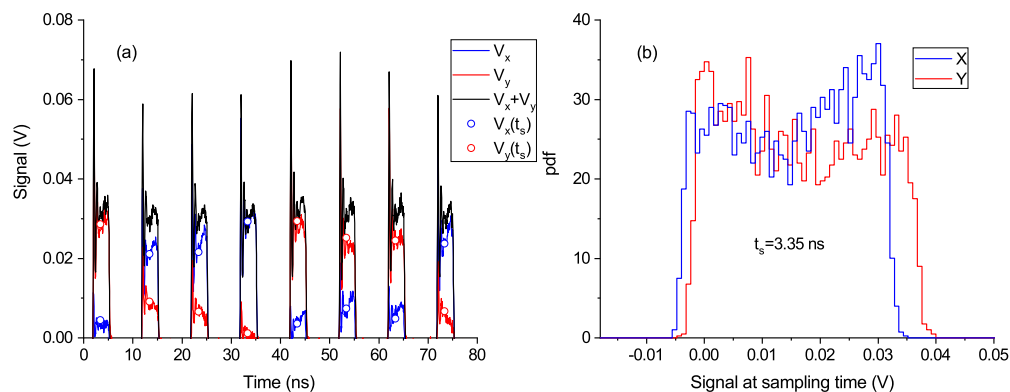


Figure 3. (a) Time traces of the signals corresponding to the x -polarization (blue line), y -polarization (red line), and total power (black line). The signals at the sampling time, 3.35 ns, are also plotted with symbols. (b) Histograms of x and y signals at the sampling time. In this figure, $T = 20\text{ }^\circ\text{C}$, $f_{\text{mod}} = 100\text{ MHz}$, $V_{\text{on}} = 0.4\text{ V}$, and $I_{\text{off}} = 2.2\text{ mA}$.

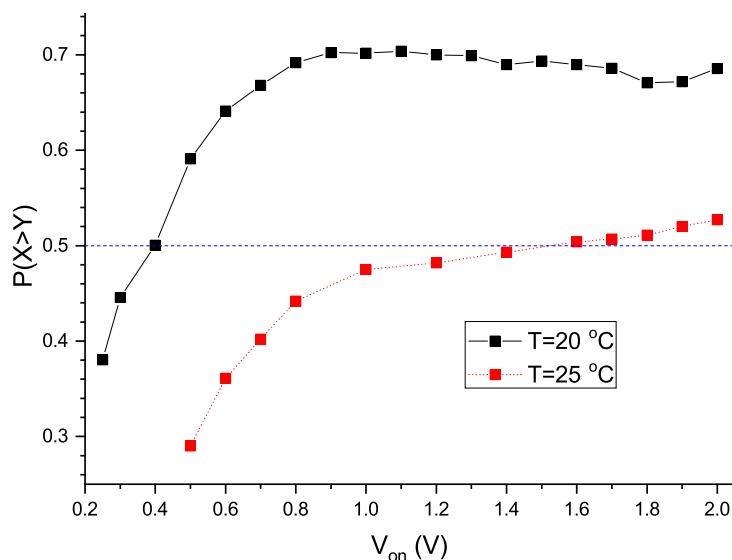


Figure 4. Probability of excitation of the x -polarization as a function of V_{on} for two different values of the temperature. In this figure, $f_{\text{mod}} = 100\text{ MHz}$, $I_{\text{off}} = 0.92I_{\text{th}}$, and $t_s = 3.35\text{ ns}$.

Figure 5 shows the histograms of the signals corresponding to both linear polarization modes at $t_s = 3.35\text{ ns}$ for several values of V_{on} when $T = 20\text{ }^\circ\text{C}$. Figure 5 shows that for small values of V_{on} , both pdfs are close to those corresponding to uniform distributions. As V_{on} increases, both pdfs evolve in such a way that the distribution corresponding to $V_x(t_s)$ develops a clear peak close to the maximum value of the signal, while the pdf of $V_y(t_s)$ develops a clear peak close to zero. Figure 5 shows that the shapes of both pdfs do not change significantly while $0.9\text{ V} \leq V_{\text{on}} \leq 1.8\text{ V}$, which is precisely the region in which saturation is observed in Figure 4 for $T = 20\text{ }^\circ\text{C}$. In fact, due to the small fluctuations of the total power, $V_x(t_s) + V_y(t_s) \sim C$, where C is constant for a given value of V_{on} . C increases from 0.075 V to 0.1 V when V_{on} changes from 0.9 V to 1.8 V. In this way, we can write that $P(X > Y) = P(V_x(t_s) > C/2)$, which remains constant in the range $0.9\text{ V} \leq V_{\text{on}} \leq 1.8\text{ V}$, in this way explaining the region of saturation of $P(X > Y)$ in Figure 4.

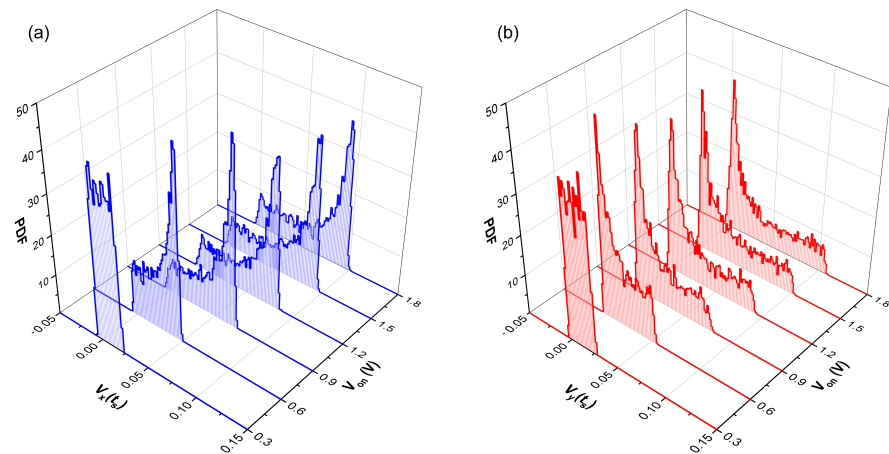


Figure 5. Histograms of the signals corresponding to (a) *x*- and (b) *y*-polarizations at the sampling time for several values of V_{on} . In this figure, $T = 20\text{ }^{\circ}\text{C}$, $f_{mod} = 100\text{ MHz}$, $I_{off} = 2.2\text{ mA}$, and $t_s = 3.35\text{ ns}$.

The previous saturation behavior is also observed when changing the sampling time, as demonstrated in Figure 6. This behavior can be explained in a similar way to that reported in Figure 5 in terms of the evolution of the pdfs of $V_x(t_s)$ and $V_y(t_s)$ for different values of t_s (not shown).

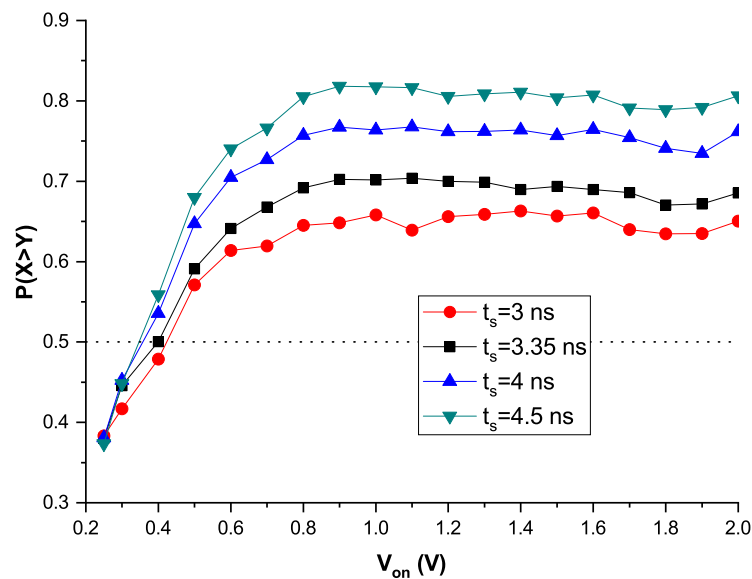


Figure 6. Probability of excitation of the *x*-polarization as a function of V_{on} for different values of the sampling time. In this figure, $T = 20\text{ }^{\circ}\text{C}$, $f_{mod} = 100\text{ MHz}$, and $I_{off} = 2.2\text{ mA}$.

We now discuss the results obtained when increasing the pulse repetition frequency to 200 MHz, which corresponds to $P = 5\text{ ns}$. Figure 7a shows the time traces corresponding to both linearly polarized modes when $T = 20\text{ }^{\circ}\text{C}$, $f_{mod} = 200\text{ MHz}$, and $V_{on} = 0.6\text{ V}$. The random excitation of both polarization modes illustrated in Figure 7a is quantified in Figure 7b, where the histograms of $V_x(t_s)$ and $V_y(t_s)$ are plotted for $t_s = 2.2\text{ ns}$. As shown in Figure 3, the modulation parameters and t_s were chosen in order to obtain pdfs of $V_x(t_s)$ and $V_y(t_s)$ with a shape close to that of a uniform distribution in such a way that $P(X > Y) = 0.517$.

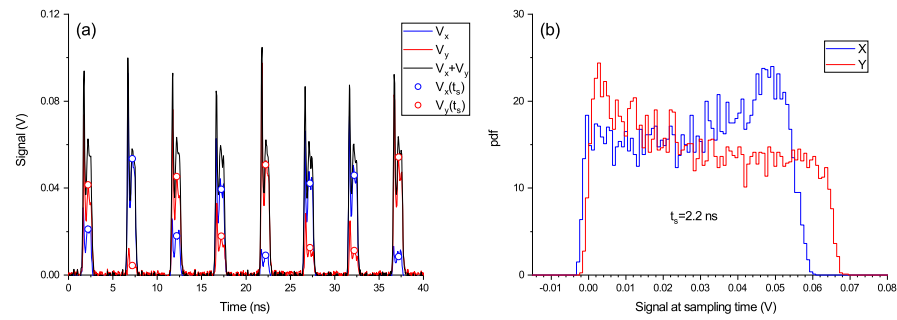


Figure 7. (a) Time traces of the signals corresponding to the x-polarization (blue line), y-polarization (red line), and total power (black line). (b) Histograms of x and y signals at the sampling time. The signals at the sampling time are plotted with circles. In this figure, $T = 20\text{ }^\circ\text{C}$, $f_{\text{mod}} = 200\text{ MHz}$, $V_{\text{on}} = 0.6\text{ V}$, $I_{\text{off}} = 2.2\text{ mA}$, and $t_s = 2.2\text{ ns}$.

The dependence of $P(X > Y)$ on V_{on} for several values of t_s when $f_{\text{mod}} = 200\text{ MHz}$ and the temperature is $20\text{ }^\circ\text{C}$ is shown in Figure 8. This figure shows that we obtain a similar qualitative behavior to that described in Figure 6 for a modulation frequency of 100 MHz . These similarities also appear when measuring $P(X > Y)$ as a function of V_{on} for several values of the temperature, as shown in Figure 9. Again, a clear saturation behavior appears when $T = 20\text{ }^\circ\text{C}$. In addition, $P(X > Y)$ increases in the considered V_{on} range when $T = 25\text{ }^\circ\text{C}$, similarly to the results included in Figure 4.

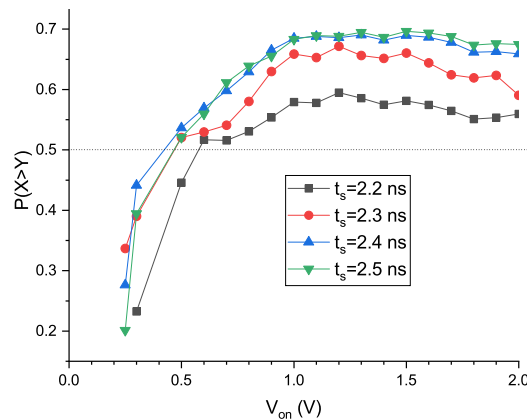


Figure 8. Probability of excitation of the x-polarization as a function of V_{on} for different values of the sampling time. In this figure, $T = 20\text{ }^\circ\text{C}$, $f_{\text{mod}} = 200\text{ MHz}$, and $I_{\text{off}} = 2.2\text{ mA}$.

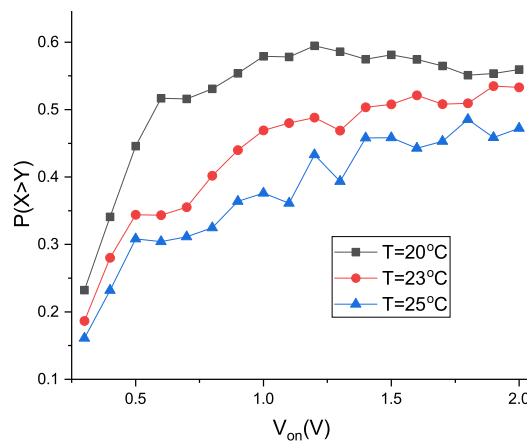


Figure 9. Probability of excitation of the x-polarization as a function of V_{on} for different values of the temperature. In this figure, $f_{\text{mod}} = 200\text{ MHz}$, $I_{\text{off}} = 0.92I_{\text{th}}$, and $t_s = 2.2\text{ ns}$.

The dependence of $P(X > Y)$ on the temperature is analyzed in Figure 10 for several values of the amplitude of the modulation for the same conditions of Figure 9. This figure shows that the probability of excitation of the x -polarization decreases with the temperature. The reasons for this dependence are discussed in the next section.

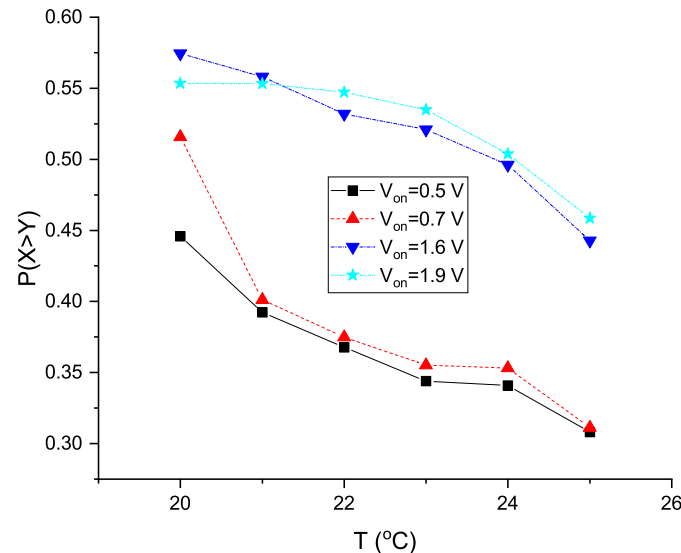


Figure 10. Probability of excitation of the x -polarization as a function of the temperature for different values of V_{on} . In this figure, $f_{mod} = 200$ MHz, $I_{off} = 0.92I_{th}$, and $t_s = 2.2$ ns.

4. Discussion and Summary

4.1. Discussion of Experimental Results

As discussed in the introduction, we expected to observe a significant effect of the temperature on the probability of excitation of a linearly polarized mode when gain-switching the VCSEL, as the temperature of the device has a large impact on its polarization properties [50,51,58,59]. This is precisely what we observed in our measurements. In addition, we showed in Figure 10 that the probability of excitation of the x -polarized mode decreases with the temperature. This dependence can be explained by considering the dependence of the effective dichroism, γ_0 , on the temperature. Our VCSEL has a Type I PS (from the shorter to the longer optical wavelength) [51] similar to those observed in [59,61] for similar devices. We recently showed that the experimental dependence of $P(X > Y)$ on V_{on} is theoretically well described with the model of [61] only when a dependence of the effective dichroism on the bias current, I , is considered [62]. This dependence has been experimentally observed [59,61] in such a way that it is approximately linear around the PS current. We theoretically obtained that $P(X > Y)$ decreases when $d\gamma_0/dI$ decreases [62]. We experimentally observed that $d\gamma_0/dI$ decreases from -660 MHz/mA to -980 MHz/mA when increasing the temperature from $T = 15$ °C [59] to $T = 25$ °C [61], respectively. This explains why $P(X > Y)$ decreases with the temperature.

The dependence of $P(X > Y)$ on the pump current at a given t_s can be explained as follows. The usual situation is that $P(X > Y)$ increases with the bias current because the x -polarized mode is favored as the current increases, as seen in Figure 2. This is, for instance, the situation observed in Figure 4 for $T = 25$ °C. A good agreement between experiments and theory is found at that temperature when we consider in the model a linear dichroism, γ_a , that decreases linearly with the bias current [62]. This situation is found in experiments for a similar device at the same temperature in the range of currents where polarization switching is observed [61]. The detailed dependence of γ_a on the current is therefore essential in determining $P(X > Y)$. A possible explanation for the saturation observed at $T = 20$ °C of $P(X > Y)$ as the current increases is that γ_a reaches a constant value in the saturation region since we theoretically obtained that $P(X > Y)$ changes only slightly with the current when γ_a is independent of the current [62]. This

could be experimentally confirmed by measuring the dependence of γ_a on the current at $T = 20^\circ\text{C}$ following the procedure explained in [61].

Since the considered modulation frequencies are well below the small signal modulation bandwidth of the VCSEL, we used the V–I curve to relate the values of V_{on} to the value of the current when V_{on} is applied, I_{on} [55,62].

The dependence of $P(X > Y)$ on t_s at a given pump current appears because random bits are obtained in each period before the steady state is reached. We proceeded in this way in order to obtain situations in which $P(X > Y)$ is close to 0.5 at high modulation frequencies. As mentioned above, the detailed dependence of $P(X > Y)$ on t_s can be described when considering the dependence of the linear birefringence on the injected current in a rate equation model. High frequencies have been considered for obtaining fast bit rates. The situation would change if much smaller modulation frequencies are considered in such a way that the VCSEL is able to reach the steady state. For the VCSEL considered in this work, in which the bistable region is very narrow, if V_{on} is large enough for the x -polarization to be the only one that emits with non-negligible power, $P(X > Y)$ would be close to 1 if t_s is chosen when the laser has reached the steady state. In this case, no dependence would be observed on t_s , but the VCSEL would not be useful to generate random numbers. At these low frequencies, using VCSELs with large bistable regions, as suggested in [52–54,56], is more interesting because $P(X > Y)$ has an intermediate value between 0 and 1 that is independent of t_s , providing that the steady state has been reached. Future work is planned in this direction.

4.2. Digitization and Post-Processing of the Data

Post-processing is necessary in RNGs because raw outputs of physical generators show deviations from the mathematical ideal of statistically independent and uniformly distributed bits [14,15]. We showed, in [46], that post-processing of the complete set of raw bits was required in order to fully pass the NIST tests. We now propose a method of obtaining the raw bits that is different to those described in [46,55]. Using this new method, the post-processing is greatly reduced. The method is based on choosing the situations for which the distributions of $V_x(t_s)$ and $V_y(t_s)$ are approximately uniform. Some examples have been already identified: Figures 3 and 5 for $V_{\text{on}} = 0.3\text{ V}$, and Figure 7. The method consists of obtaining random numbers, u , between 0 and 1 in the following way. We consider $V_{x,2}$ ($V_{x,1}$) as a value that is slightly smaller (larger) than the maximum (minimum) value of $V_x(t_s)$. If $V_{x,1} < V_x(t_s) < V_{x,2}$, we calculate $u = V_x(t_s)/(V_{x,2} - V_{x,1})$; otherwise, we do not use $V_x(t_s)$ to calculate u . We also obtain u numbers from $V_y(t_s)$, exchanging x for y in the previous expressions.

The results of this procedure are shown in Figure 11, where the pdf corresponding to the u -values obtained from the data of Figure 7 is shown. In obtaining this figure, we used $(V_{x,1}, V_{x,2}) = (-0.00076, 0.054)$, $(V_{y,1}, V_{y,2}) = (-0.00016, 0.065)$, 10^4 values of $V_x(t_s)$, and 10^4 values of $V_y(t_s)$. In this way, 19,236 u -values were used to plot the histogram of Figure 11 (only 3.8% of the data were discarded). Figure 11 shows that the distribution of u -values is approximately uniform. We obtained digital bits from the u -data by converting the integer part of $u 2^{27}$ into a binary number. In this way, we obtained 519,372 bits. Defining the bias, e , as $e = p(0) - 1/2$, where $p(0)$ is the probability of obtaining a “0” bit in the string, we obtained $e = 3.44 \times 10^{-4}$ for our data.

Table 1 shows the results obtained with the NIST statistical test applied to our bit string. Each test was performed using 519 sequences of 1000 bits, each with a statistical significance level $\alpha = 0.01$. If the bits are random, mean p -values must be close to 0.5 and the proportions of sequences that pass the test must be in the interval $[0.9768, 1]$ [57]. Table 1 shows that our bits are sufficiently random for passing the considered statistical test of NIST. We did not consider all the NIST test because our bit number was small. In this way, we only calculated the proportions of sequences for those tests that can work with short bit strings. Our results try to demonstrate that certain levels of randomness can be achieved when directly using the raw data and a minimum level of post-processing. In our case,

the post-processing consisted just of evaluating if the raw data were in a certain interval. For our bit string, we obtained a high accepted bit rate of 96.2%.

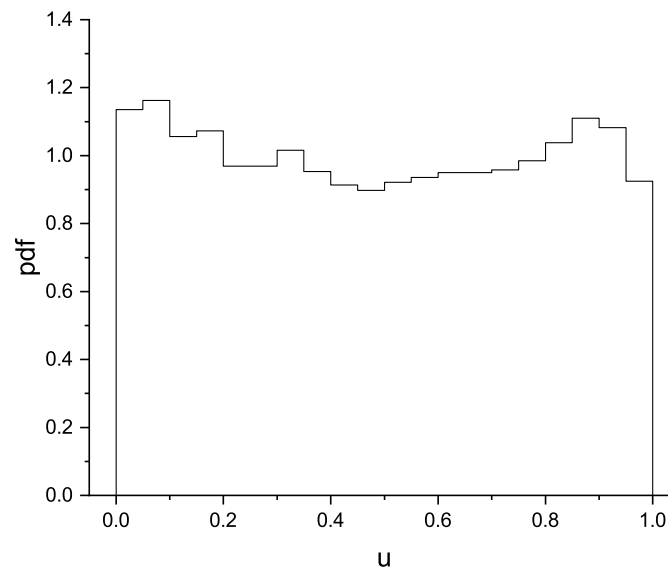


Figure 11. Normalized histogram of data corresponding to Figure 7b.

Table 1. Output of NIST test.

Test	Mean <i>p</i> -Value	Proportion Pass
Frequency	0.479	0.985
Block frequency	0.490	0.992
Run	0.488	0.990
Longest run	0.486	0.990
DFT	0.490	0.979
Cumulative sums forw.	0.507	0.988
Cumulative sums back.	0.495	0.990

Our number of bits was small so the question of whether all the NIST tests are fully passed with sufficient number of data still remains. We showed in this paper that the probability of excitation of a linear polarization significantly depends on the VCSEL temperature. This means that some bias can appear due to unwanted and slight variations of the temperature. The situation is similar with respect to slight variations of the modulation parameters. Taking into account that uniform distributions such as those observed in Figures 3, 5 and 7 only appear for rather specific values of parameters such as the applied current, temperature, and sampling time, we would expect that NIST tests could be only fully passed if a large stability of those parameters over long periods of operation is achieved. We note that NIST tests were not fully passed when using low-bias raw bits obtained with a different method [46]. In the same way, we would expect the same result with the method proposed in this section. Regardless, usual post-processing of the raw bits can be applied for fully passing the NIST test, as carried out in [46,56]. In any case, we remark that passing the NIST test is not a confirmation of true randomness or “quantumness”. There is, however, an advantage of obtaining random bits as we achieved in this section. The bit rate obtained, 10.4 Gbps ($2 \times 27 \times 2 \cdot 10^8 \times 0.962$, corresponding to the number of polarizations, bits/data, f_{mod} , and accepted bit rate, respectively) is larger than 0.1–0.2 Gbps in [46,55], in which only one bit per period was obtained.

The method described in this work to obtain a uniform pdf is not a randomness extractor. The random bits obtained in this way can be used in Monte Carlo simulations. The use of these bits for cryptographic purposes would require further post-processing,

for instance, such as that performed in [56]. We note that the choice of a uniform distribution density of the raw sequence may not be the best choice for cryptographic applications. The probability of intermediate values of the signal is appreciable, the proportion of pulses affected by classical (nonquantum) noises of the detector can be significant, and “0”-s and “1”-s resulting from the digitization of such pulses can be considered as “untrusted” bits [56]. The quantum reduction factor, which contains information on the amount of classical noise falling into the digitized random sequence due to fluctuations in the photodetector [56], would increase. The value of the quantum reduction factor also determines how much the raw random sequence should be “compressed” using a randomness extractor [56]. A better choice to decrease the quantum reduction factor would be using pdfs with two well-defined maxima, similar to those obtained in [55], for a better operation of the VCSEL in the context of QRNG [56]. Future work will be devoted to measurements using VCSELs with a large polarization bistable region for which a small quantum reduction factor is expected. In any case, post-processing of the raw bits is required for cryptographic applications. For instance, a combination of an FIR-filtering method [38,56] with random Boolean Toeplitz matrices was recently proposed in [56].

In summary, we experimentally analyzed the effect of the temperature on the probability of excitation of a linearly polarized mode when gain-switching the VCSEL. We showed that this probability significantly depends on the value of the temperature of the device. We also showed that for low values of the temperature, the probability of excitation saturates to a constant value as the amplitude of the modulation increases. We identified situations in which the distributions of the linearly polarized signals at a sampling time are approximately uniform. For these situations, we discussed the randomness of our data by using the NIST statistical test.

Funding: This research was funded by Ministerio de Ciencia e Innovación, Spain, under grant PID2021-123459OB-C22 MICN/AEI/10.13039/501100011033/FEDER, UE. A. Quirce acknowledges financial support from Beatriz Galindo program, Ministerio de Ciencia, Innovación y Universidades (Spain).

Conflicts of Interest: The authors declare no conflicts of interest.

Abbreviations

The following abbreviations are used in this manuscript:

QRNG	Quantum random number generation
QKD	Quantum key distribution
VCSEL	Vertical-cavity surface-emitting laser
PDF	Probability density function
RNG	Random number generation
RF	Radio frequency
PS	Polarization switching
NIST	National Institute of Standards and Technology

References

1. Lax, M. Quantum noise. IV. Quantum theory of noise sources. *Phys. Rev.* **1966**, *145*, 110. [[CrossRef](#)]
2. Lax, M.; Louisell, W. Quantum noise. XII. Density-operator treatment of field and population fluctuations. *Phys. Rev.* **1969**, *185*, 568. [[CrossRef](#)]
3. Risken, H. Fokker-Planck equation. In *The Fokker-Planck Equation*; Springer: Berlin/Heidelberg, Germany, 1996.
4. Henry, C.H.; Kazarinov, R.F. Quantum noise in photonics. *Rev. Mod. Phys.* **1996**, *68*, 801. [[CrossRef](#)]
5. Arecchi, F.; Degiorgio, V.; Querzola, B. Time-dependent statistical properties of the laser radiation. *Phys. Rev. Lett.* **1967**, *19*, 1168. [[CrossRef](#)]
6. Coldren, L.A.; Corzine, S.W.; Mashanovitch, M.L. *Diode Lasers and Photonic Integrated Circuits*; John Wiley & Sons: Hoboken, NJ, USA, 2012; Volume 218.
7. Agrawal, G.P.; Dutta, N.K. *Semiconductor Lasers*; Springer Science & Business Media: Berlin/Heidelberg, Germany, 2013.
8. Henry, C. Phase noise in semiconductor lasers. *J. Light. Technol.* **1986**, *4*, 298–311. [[CrossRef](#)]

9. Balle, S.; De Pasquale, F.; Abraham, N.; San Miguel, M. Statistics of the transient frequency modulation in the switch-on of a single-mode semiconductor laser. *Phys. Rev. A* **1992**, *45*, 1955. [\[CrossRef\]](#)
10. Spano, P.; D'Ottavi, A.; Mecozzi, A.; Daino, B. Experimental observation of time jitter in semiconductor laser turn-on. *Appl. Phys. Lett.* **1988**, *52*, 2203–2204. [\[CrossRef\]](#)
11. Mecozzi, A.; Piazzolla, S.; D'Ottavi, A.; Spano, P. Passage time statistics in semiconductor laser turn on. *Phys. Rev. A* **1988**, *38*, 3136. [\[CrossRef\]](#)
12. Obermann, K.; Kindt, S.; Petermann, K. Turn-on jitter in zero-biased single-mode semiconductor lasers. *IEEE Photonics Technol. Lett.* **1996**, *8*, 31–33. [\[CrossRef\]](#)
13. Mecozzi, A.; Sapia, A.; Spano, P.; Agrawal, G.P. Transient multimode dynamics in nearly single-mode lasers. *IEEE J. Quantum Electron.* **1991**, *27*, 332–343. [\[CrossRef\]](#)
14. Stipčević, M.; Koç, Ç.K. True random number generators. In *Open Problems in Mathematics and Computational Science*; Springer: Berlin/Heidelberg, Germany, 2014; pp. 275–315.
15. Herrero-Collantes, M.; Garcia-Escartin, J.C. Quantum random number generators. *Rev. Mod. Phys.* **2017**, *89*, 015004. [\[CrossRef\]](#)
16. Mannalath, V.; Mishra, S.; Pathak, A. A comprehensive review of quantum random number generators: Concepts, classification and the origin of randomness. *arXiv* **2022**, arXiv:2203.00261.
17. Lucamarini, M.; Yuan, Z.L.; Dynes, J.F.; Shields, A.J. Overcoming the rate–distance limit of quantum key distribution without quantum repeaters. *Nature* **2018**, *557*, 400–403. [\[CrossRef\]](#)
18. Bhaskar, M.K.; Riedinger, R.; Machielse, B.; Levonian, D.S.; Nguyen, C.T.; Knall, E.N.; Park, H.; Englund, D.; Lončar, M.; Sukachev, D.D.; et al. Experimental demonstration of memory-enhanced quantum communication. *Nature* **2020**, *580*, 60–64. [\[CrossRef\]](#) [\[PubMed\]](#)
19. Xie, Y.M.; Lu, Y.S.; Weng, C.X.; Cao, X.Y.; Jia, Z.Y.; Bao, Y.; Wang, Y.; Fu, Y.; Yin, H.L.; Chen, Z.B. Breaking the rate-loss bound of quantum key distribution with asynchronous two-photon interference. *PRX Quantum* **2022**, *3*, 020315. [\[CrossRef\]](#)
20. Clivati, C.; Meda, A.; Donadello, S.; Virzì, S.; Genovese, M.; Levi, F.; Mura, A.; Pittaluga, M.; Yuan, Z.; Shields, A.J.; et al. Coherent phase transfer for real-world twin-field quantum key distribution. *Nat. Commun.* **2022**, *13*, 157. [\[CrossRef\]](#)
21. Gu, J.; Cao, X.Y.; Fu, Y.; He, Z.W.; Yin, Z.J.; Yin, H.L.; Chen, Z.B. Experimental measurement-device-independent type quantum key distribution with flawed and correlated sources. *Sci. Bull.* **2022**, *67*, 2167–2175. [\[CrossRef\]](#)
22. Yin, H.L.; Fu, Y.; Li, C.L.; Weng, C.X.; Li, B.H.; Gu, J.; Lu, Y.S.; Huang, S.; Chen, Z.B. Experimental quantum secure network with digital signatures and encryption. *Natl. Sci. Rev.* **2022**, nwac228. [\[CrossRef\]](#)
23. Paraíso, T.K.; Woodward, R.I.; Marangon, D.G.; Lovic, V.; Yuan, Z.; Shields, A.J. Advanced Laser Technology for Quantum Communications (Tutorial Review). *Adv. Quantum Technol.* **2021**, *4*, 2100062. [\[CrossRef\]](#)
24. Shalm, L.K.; Zhang, Y.; Bienfang, J.C.; Schlager, C.; Stevens, M.J.; Mazurek, M.D.; Abellán, C.; Amaya, W.; Mitchell, M.W.; Alhejji, M.A.; et al. Device-independent randomness expansion with entangled photons. *Nat. Phys.* **2021**, *17*, 452–456. [\[CrossRef\]](#)
25. Liu, W.B.; Lu, Y.S.; Fu, Y.; Huang, S.C.; Yin, Z.J.; Jiang, K.; Yin, H.L.; Chen, Z.B. Source-independent quantum random number generator against tailored detector blinding attacks. *Opt. Express* **2023**, *31*, 11292–11307. [\[CrossRef\]](#)
26. Jennewein, T.; Achleitner, U.; Weihs, G.; Weinfurter, H.; Zeilinger, A. A fast and compact quantum random number generator. *Rev. Sci. Instrum.* **2000**, *71*, 1675–1680. [\[CrossRef\]](#)
27. Stipčević, M.; Rogina, B.M. Quantum random number generator based on photonic emission in semiconductors. *Rev. Sci. Instrum.* **2007**, *78*, 045104. [\[CrossRef\]](#) [\[PubMed\]](#)
28. Wei, W.; Guo, H. Bias-free true random-number generator. *Opt. Lett.* **2009**, *34*, 1876–1878. [\[CrossRef\]](#)
29. Fürst, H.; Weier, H.; Nauwerth, S.; Marangon, D.G.; Kurtsiefer, C.; Weinfurter, H. High speed optical quantum random number generation. *Opt. Express* **2010**, *18*, 13029–13037. [\[CrossRef\]](#)
30. Durt, T.; Belmonte, C.; Lamoureux, L.P.; Panajotov, K.; Van den Berghe, F.; Thienpont, H. Fast quantum-optical random-number generators. *Phys. Rev. A* **2013**, *87*, 022339. [\[CrossRef\]](#)
31. Guo, H.; Tang, W.; Liu, Y.; Wei, W. Truly random number generation based on measurement of phase noise of a laser. *Phys. Rev. E* **2010**, *81*, 051137. [\[CrossRef\]](#)
32. Shen, Y.; Tian, L.; Zou, H. Practical quantum random number generator based on measuring the shot noise of vacuum states. *Phys. Rev. A* **2010**, *81*, 063814. [\[CrossRef\]](#)
33. Qi, B.; Chi, Y.M.; Lo, H.K.; Qian, L. High-speed quantum random number generation by measuring phase noise of a single-mode laser. *Opt. Lett.* **2010**, *35*, 312–314. [\[CrossRef\]](#)
34. Jofre, M.; Curty, M.; Steinlechner, F.; Anzolin, G.; Torres, J.; Mitchell, M.; Pruneri, V. True random numbers from amplified quantum vacuum. *Opt. Express* **2011**, *19*, 20665–20672. [\[CrossRef\]](#)
35. Argyris, A.; Pikasis, E.; Deligiannidis, S.; Syvridis, D. Sub-Tb/s physical random bit generators based on direct detection of amplified spontaneous emission signals. *J. Light. Technol.* **2012**, *30*, 1329–1334. [\[CrossRef\]](#)
36. Xu, F.; Qi, B.; Ma, X.; Xu, H.; Zheng, H.; Lo, H.K. Ultrafast quantum random number generation based on quantum phase fluctuations. *Opt. Express* **2012**, *20*, 12366–12377. [\[CrossRef\]](#) [\[PubMed\]](#)
37. Abellán, C.; Amaya, W.; Jofre, M.; Curty, M.; Acín, A.; Capmany, J.; Pruneri, V.; Mitchell, M. Ultra-fast quantum randomness generation by accelerated phase diffusion in a pulsed laser diode. *Opt. Express* **2014**, *22*, 1645–1654. [\[CrossRef\]](#)
38. Yuan, Z.; Lucamarini, M.; Dynes, J.; Fröhlich, B.; Plews, A.; Shields, A. Robust random number generation using steady-state emission of gain-switched laser diodes. *Appl. Phys. Lett.* **2014**, *104*, 261112. [\[CrossRef\]](#)

39. Nie, Y.Q.; Huang, L.; Liu, Y.; Payne, F.; Zhang, J.; Pan, J.W. The generation of 68 Gbps quantum random number by measuring laser phase fluctuations. *Rev. Sci. Instrum.* **2015**, *86*, 063105. [[CrossRef](#)] [[PubMed](#)]
40. Abellan, C.; Amaya, W.; Domenech, D.; Muñoz, P.; Capmany, J.; Longhi, S.; Mitchell, M.W.; Pruneri, V. Quantum entropy source on an InP photonic integrated circuit for random number generation. *Optica* **2016**, *3*, 989–994. [[CrossRef](#)]
41. Marangon, D.G.; Plews, A.; Lucamarini, M.; Dynes, J.F.; Sharpe, A.W.; Yuan, Z.; Shields, A.J. Long-term test of a fast and compact quantum random number generator. *J. Light. Technol.* **2018**, *36*, 3778–3784. [[CrossRef](#)]
42. Septriani, B.; de Vries, O.; Steinlechner, F.; Gräfe, M. Parametric study of the phase diffusion process in a gain-switched semiconductor laser for randomness assessment in quantum random number generator. *AIP Adv.* **2020**, *10*, 055022. [[CrossRef](#)]
43. Shakhovoy, R.; Sych, D.; Sharoglazova, V.; Udaltsov, A.; Fedorov, A.; Kurochkin, Y. Quantum noise extraction from the interference of laser pulses in an optical quantum random number generator. *Opt. Express* **2020**, *28*, 6209–6224. [[CrossRef](#)]
44. Shakhovoy, R.; Sharoglazova, V.; Udaltsov, A.; Duplinskiy, A.; Kurochkin, V.; Kurochkin, Y. Influence of Chirp, Jitter, and Relaxation Oscillations on Probabilistic Properties of Laser Pulse Interference. *IEEE J. Quantum Electron.* **2021**, *57*, 1–7. [[CrossRef](#)]
45. Lovic, V.; Marangon, D.G.; Lucamarini, M.; Yuan, Z.; Shields, A.J. Characterizing Phase Noise in a Gain-Switched Laser Diode for Quantum Random-Number Generation. *Phys. Rev. Appl.* **2021**, *16*, 054012. [[CrossRef](#)]
46. Valle-Miñón, M.; Quirce, A.; Valle, A.; Gutiérrez, J. Quantum random number generator based on polarization switching in gain-switched VCSELs. *Opt. Contin.* **2022**, *1*, 2156–2166. [[CrossRef](#)]
47. Alarcón, A.; Argillander, J.; Spegel-Lexne, D.; Xavier, G. Dynamic generation of photonic spatial quantum states with an all-fiber platform. *Opt. Express* **2023**, *31*, 10673–10683. [[CrossRef](#)]
48. Loudon, R. *The Quantum Theory of Light*; OUP Oxford: Oxford, UK, 2000.
49. Aldama, J.; Sarmiento, S.; Etcheverry, S.; Valivarathi, R.; Grande, I.L.; Vidarte, L.T.; Pruneri, V. Small-form-factor Gaussian-modulated coherent-state transmitter for CV-QKD using a gain-switched DFB laser. *Opt. Express* **2023**, *31*, 5414–5425. [[CrossRef](#)]
50. Choquette, K.D.; Schneider, R.P.; Lear, K.L.; Leibenguth, R.E. Gain-dependent polarization properties of vertical-cavity lasers. *IEEE J. Sel. Top. Quantum Electron.* **1995**, *1*, 661–666. [[CrossRef](#)]
51. Michalzik, R. *VCSELs: Fundamentals, Technology and Applications of Vertical-Cavity Surface-Emitting Lasers*; Springer: Berlin/Heidelberg, Germany, 2012; Volume 166.
52. Chizhevsky, V. Bistable vertical cavity laser with periodic pump modulation as a random bits generator. *Opt. Spectrosc.* **2010**, *108*, 343–346. [[CrossRef](#)]
53. Zhao, J.; Li, P.; Zhang, X.; Gao, Z.; Jia, Z.; Bogris, A.; Shore, K.A.; Wang, Y. Fast all-optical random number generator. *arXiv* **2022**, arXiv:2201.07616.
54. Shakhovoy, R.; Maksimova, E.; Sharoglazova, V.; Puplauskis, M.; Kurochkin, Y. Fast and compact VCSEL-based quantum random number generator. *J. Phys. Conf. Ser.* **2021**, *1984*, 012005. [[CrossRef](#)]
55. Quirce, A.; Valle, A. Random polarization switching in gain-switched VCSELs for quantum random number generation. *Opt. Express* **2022**, *30*, 10513–10527. [[CrossRef](#)]
56. Shakhovoy, R.; Maksimova, E. Gain-switched VCSEL as a quantum entropy source: The problem of quantum and classical noise. *St. Petersburg Polytechnic Univ. J. Phys. Math.* **2022**, *15*, 201–205.
57. Rukhin, A.; Soto, J.; Nechvatal, J.; Smid, M.; Barker, E.; Leigh, S.; Levenson, M.; Vangel, M.; Banks, D.; Heckert, A.; et al. NIST Special Publication 800-22: A statistical test suite for the validation of random number generators and pseudo random number generators for cryptographic applications. *NIST Spec. Publ.* **2010**, *800*, 22.
58. Ryvkin, B.; Georgievski, A. Effect of photon-energy-dependent loss and gain mechanisms on polarization switching in vertical-cavity surface-emitting lasers. *JOSA B* **1999**, *16*, 2106–2113. [[CrossRef](#)]
59. Quirce, A.; Valle, A.; Pesquera, L.; Thienpont, H.; Panajotov, K. Measurement of temperature-dependent polarization parameters in long-wavelength VCSELs. *IEEE J. Sel. Top. Quantum Electron.* **2015**, *21*, 636–642. [[CrossRef](#)]
60. Valle, A.; Sciamanna, M.; Panajotov, K. Irregular pulsating polarization dynamics in gain-switched vertical-cavity surface-emitting lasers. *IEEE J. Quantum Electron.* **2008**, *44*, 136–143. [[CrossRef](#)]
61. Pérez, P.; Valle, A.; Pesquera, L. Polarization-resolved characterization of long-wavelength vertical-cavity surface-emitting laser parameters. *J. Opt. Soc. Am. B* **2014**, *31*, 2574–2580. [[CrossRef](#)]
62. Quirce, A.; Valle, A.; Valle-Miñón, M.; Gutiérrez, J. Characterizing polarization switching in gain-switched vertical-cavity surface-emitting lasers for quantum random number generation. In Proceedings of the European Quantum Electronics Conference, Virtual, 26–30 June 2023; p. EB-P.8.

Disclaimer/Publisher’s Note: The statements, opinions and data contained in all publications are solely those of the individual author(s) and contributor(s) and not of MDPI and/or the editor(s). MDPI and/or the editor(s) disclaim responsibility for any injury to people or property resulting from any ideas, methods, instructions or products referred to in the content.